LABORATOIRE DE PHYSIQUE CORPUSCULAIRE

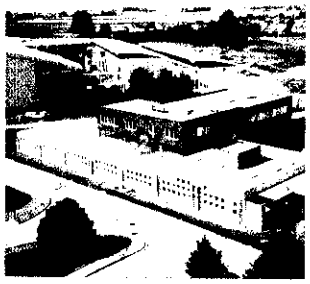

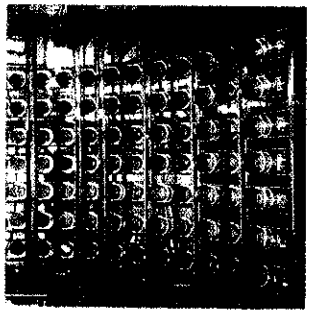

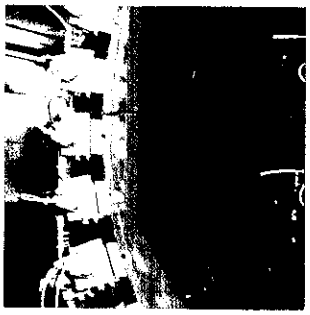

TONNERRE: An Array for Delayed-Neutron Decay Spectroscopy

A. Buţă, T. Martin, C. Timiş, N. Achouri, J.C. Angélique, C. Borcea, I. Cruceru, A. Genoux-Lubain, S. Grévy, M. Lewitowicz, E. Lienard, F.M. Marqués, F. Negoiţă, F. de Oliveira, N.A. Orr, J. Péter, M. Sandu

October 1999

LPCC 99-22

Submitted to NIM A

CENTRE NATIONAL DE LA RECHERCHE SCIENTIFIQUE

INSTITUT NATIONAL
DE PHYSIQUE NUCLÉAIRE ET DE PHYSIQUE DES PARTICULES

INSTITUT DES SCIENCES DE LA MATIÈRE ET DU RAYONNEMENT

UNIVERSITÉ DE CAEN

- U.M.R.6534 -
ISMRA - 6, Boulevard Maréchal Juin - 14050 CAEN CEDEX - FRANCE

Téléphone : 02 31 45 25 00 - Télécopie : 02 31 45 25 49
Internet : http://caeinfo.in2p3.fr

1 Introduction

Decay studies provide one of the primary spectroscopic tools for the investigation of nuclei far from stability. The large β-decay energy for such nuclei often leads to the population of particle-unbound states in the daughter. As a result, β-delayed particle emission is frequently the dominant decay mode [1]. Access to the location and structure of unbound levels thus requires the measurement of the delayed particles-in particular the energies. More generally such information is essential to the mapping of the β-strength function of nuclei far from stability. For very neutron-rich nuclei, delayed neutron emission occurs, with delayed multi-neutron emission taking place in many cases.

Early measurements of β-delayed neutron emission [2–9] used energy-integrated detectors which provided for determinations of half-lives and neutron emission probabilities (P_n) and as such allowed the decay modes to be established. In order to proceed further in the extraction of spectroscopic information, Huck *et al* [10] constructed two large area plastic detectors for neutron time-of-flight spectrometry and were able to measure β-delayed neutron energies following the decay of neutron rich K, Ca and Sc nuclei at ISOLDE. More recently, Harkewicz *et al* [11] constructed a 16 element time-of-flight spectrometer also based on plastic scintillators and using the A1200 fragment separator at MSU was able to resolve several neutron unbound states in ^{15}C, populated in the β-decay of ^{15}B. This device has also been used to study the β-delayed neutron emission in the decays of ^{18}N [12], $^{17,18}C$ [13] and ^{11}Li [14]. The case of ^{11}Li demonstrates the utility of such measurements since the branching ratios for emitting one and two neutrons are 85 % and 4 % respectively: only two bound states are fed in ^{11}Be. It should also be noted that similar detector arrays are in use at RIKEN [15,16].

The primary difficulty in working with radioactive beams (RNB) are the very weak intensities (typically $\sim$ 1-10^3 pps) compared to beams of stable nuclei ($\sim 10^{11}$ pps). Clearly then, the decay spectroscopy of very neutron-rich nuclei requires a neutron detection system of high efficiency (particularly for energies below $\sim$ 5 MeV), good energy and angular resolution and a granularity sufficient to provide for the detection of multi-neutron decays. Such needs are met by a system with a high intrinsic efficiency, large acceptance and modular construction. The weak point of most existing devices is the small overall efficiency, defined as the product of the intrinsic efficiency of one detector module, ϵ_n and the solid angle $\Delta\Omega$ of the array.

Here we report on the design and construction of the detector array TONNERRE (TONneau pour NEutRons REtardes). The aim was to build a detector which, compared to similar devices, should have a better overall efficiency but comparable granularity and energy resolution. The following section

TONNERRE: An Array for Delayed-Neutron Decay Spectroscopy

A. Buţă [a,b], T. Martin [a], C. Timiş [b], N. Achouri [a], J.C. Angélique [a], C. Borcea [b], I. Cruceru [b], A. Genoux-Lubain [d], S. Grévy [a], M. Lewitowicz [c], E. Lienard [a], F.M. Marqués [a], F. Negoiţă [b], F. de Oliveira [c], N.A. Orr [a], J. Péter [a] and M. Sandu [b]

[a] *Laboratoire de Physique Corpusculaire, IN2P3-CNRS, ISMRA et Université de Caen, Boulevard Maréchal Juin, 14050 CAEN Cedex,FRANCE*

[b] *National Institute for Physics and Nuclear Engineering, P.O. Box MG-6, BUCHAREST, ROMANIA*

[c] *GANIL, CEA/DSM-CNRS/IN2P3, BP 5027, 14076 CAEN Cedex, FRANCE*

[d] *Laboratoire de Physique Corpusculaire, IN2P3-CNRS et Université de Clermont-Ferrand, 24 Avenue des Landais, 63177, AUBIERE, FRANCE*

Abstract

The design and construction of an array for delayed-neutron decay spectroscopy is presented. The array is composed of 32 plastic scintillator (BC400) modules which each provide for time-of-flight (energy) and position measurements. The intrinsic detection efficiency is 30% at E_n=2 MeV and the resolution $\delta E_n/E_n \sim 10\%$ (FWHM). The array can cover a total solid angle of up to 50% of 4π. Details of studies performed to optimize the performances of the individual modules are reported, as well as source testing and in-beam commissioning.

Key words: Neutron detector array, plastic scintillators, time-of-flight, β-delayed neutron spectroscopy, neutron-rich nuclei.
PACS: 29.40.Mc; 29.30.Hs; 21.10.-k

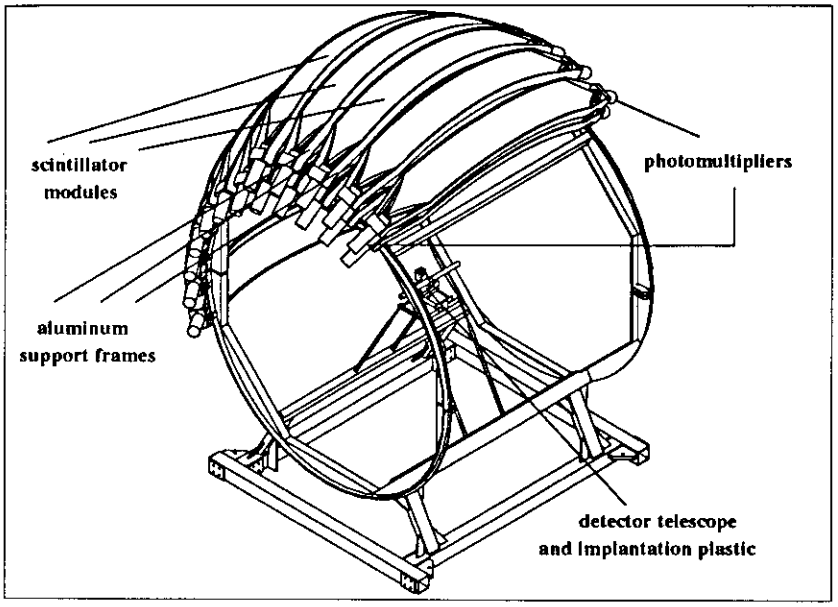

Fig. 1. General view of the TONNERRE array.

the same flight path for all neutrons. A radius of 120 cm was chosen as a compromise between the energy resolution, total solid angle and mechanical integrity. From a practical point of view, the overall size of the array is such that it can be installed at various RNB facilities.

The elements of the array are viewed at both ends by PMT's and can be arranged in two layers in order to boost the intrinsic efficiency. The start for the TOF measurement is provided by the detection of the decay electrons in an implantation detector located at the center of the array-typically a small scintillator block viewed by two PMT's.
The material chosen for the individual detector elements, plastic scintillator, is transparent to its own light output, has a fast response and can be made easily in different shapes and sizes. For the current project BC400 [1], which has an intrinsic decay time of 2.4 ns, a light output 65 % that of anthracene, a bulk attenuation length of 250 cm and a H to C ratio of 1.1, was chosen. The PMT's used are XP2262 (2 in) tubes. The spectral sensitivity of these PMT's peaks at 420 nm and thus matches very well the wavelength of maximal emission of BC400 (423 nm).

The considerations described here defined the basic design of the detector. Detailed Monte-Carlo simulations and light attenuation measurements were, however, required to optimize the dimensions of the detector modules.

[1] †Fabricated by BICRON

describes the preliminary studies which led to the final design for TONNERRE-32 thick scintillator bars, 160x20x4 cm^3, bent to a radius of curvature (the flight path) of 120 cm and viewed at both ends by photomultiplier tubes (PMT). In section 3 the properties and performances of the detector are presented, whilst section 4 describes the first in-beam tests at GANIL with ^{15}B, ^{16}C and ^{17}N. Some conclusions and perspectives for future work are given in section 5.

2 Design studies

2.1 General considerations

Two basic problems are encountered in the measurement of neutron kinetic energies with high intrinsic efficiency and very good resolution.

Firstly, almost all methods of detecting neutrons involve imparting some or all of the neutron's kinetic energy to a (charged) nucleus which is then detected. Thus, for high intrinsic efficiency a detector is required with a total thickness of several times the neutron interaction length: ~14 cm for neutrons of several MeV in typical scintillator materials [17]. A high intrinsic efficiency therefore requires the use of relatively thick detectors.

Secondly, high resolution measurements of neutron kinetic energies are only feasible by means of time-of-flight (TOF) methods. Generally, organic scintillators are used for this purpose since they provide for good timing and, hence, energy resolution. The energy resolution is given by,

$$\frac{\delta E}{E} = 2\left[\left(\frac{\delta d}{d}\right)^2 + \left(\frac{\delta T}{T}\right)^2\right]^{1/2} \qquad (1)$$

where d is the flight path, T the flight time, δd and δT the respective resolutions (FWHM). For infinitely good time resolution (δT=0), the energy resolution is limited by the finite detector thickness Δd, since the interaction can occur anywhere within the detector. A detector of 2 cm thickness contributes 4% to the energy resolution if the flight path is 1 m. Thus, precise TOF measurements require rather thin detectors.

In order to meet both the requirement of a good energy resolution and that of a resonnable overall efficiency, the technical solution retained for our neutron detector array is the following: a barrel like geometry constituted of individual plastic scintillator detectors (Fig. 1), curved to the same radius to ensure

The region of constant attenuation between -60 and 60 cm is clearly apparent as is the decrease in the attenuation if the light is emitted close to a PMT or at the opposite end. The simulations made with the code Guide7 from CERN [18] and with a programme written by us [17], which simulates the light propagation in two dimensions, have shown that the behaviour of the attenuation curve is due to the wedge shape ends of the module. The form of the attenuation curve is the same for both a curved and a flat scintillator.

Next, by way of simulations, we optimized the scintillator thickness using the programme developed to simulate the light propagation. The programme takes into account the exponential light attenuation inside the scintillator (specified by the manufacturer) as well as the light attenuation corresponding to reflections. This last coefficient, R, indicating imperfect total reflection (R<1) caused by scattering effects, is a function of the wavelengh, the emission angle and of the quality of the reflecting surface [19]. For example, for λ=458 nm the reflection coefficient has the expression,

$$R = -0.0055\theta_r + 0.9975 \tag{2}$$

with θ_r in degrees. The ratio of the intensities of transmitted to emitted light, taking into account both, the attenuation by reflections and the exponential attenuation can be written as,

$$\frac{J_t}{J_e} = R(\theta_r, \lambda)^N e^{-L(\theta_r)/L_a} \tag{3}$$

where L_a is the attenuation length, $L(\theta_r)$ the optical path length for an angle of emission θ_r (the angle between the reflected beam and the surface) and N is the number of reflections.
From (3) it follows that the quantity of transmitted light is optimum when the attenuation is minimum, i.e., when the number of reflections N is a minimum. Fig. 3 shows the number of reflections and the ratio of the transmitted to emitted light as a function of the scintillator thickness for a scintillator length of 160 cm and a reflection coefficient of 0.95.

The number of reflections decreases rapidly with scintillator thickness and becomes almost constant ($\sim$ 5) for thicknesses greater than 4 cm. Thus, a thickness of 4 cm was chosen-a compromise providing for a good TOF resolution (see section 2.1), an optimum light transmission and a high intrinsic efficiency. The final dimensions thus chosen for the scintillator were: total lengh 160 cm, width 20 cm and thickness 4 cm. The width of 20 cm corresponds to an uncertainty in the localization ($\pm$ 10 cm) comparable with the position resolution along the scintillator, as shown below.

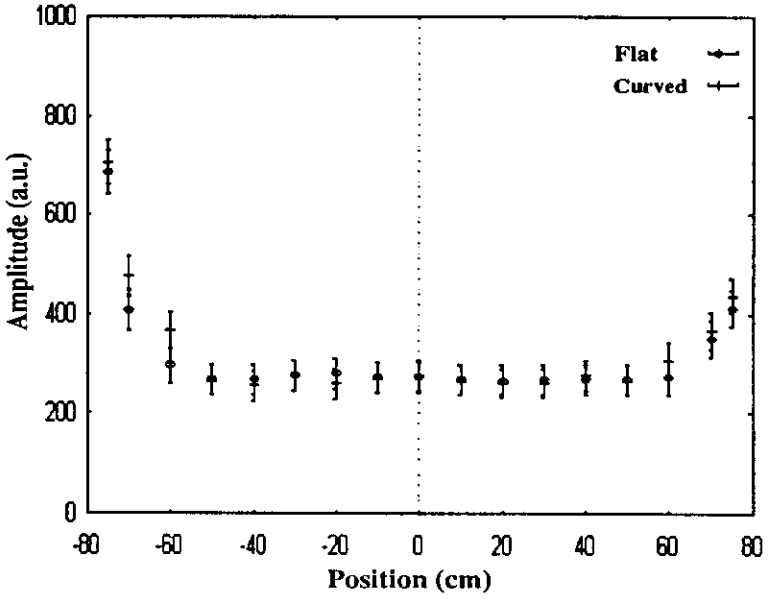

Fig. 2. Measured attenuation curve for one module, prior to and following being curved to a radius of 120 cm.

2.2 Attenuation measurements and simulations

The conditions for the scintillator light collection greatly affect timing and consequently the energy resolution. Light attenuation also affects the performances of the detector, particularly the efficiency, as, depending on the optical path length for photons, the amplitude may become lower then the detection threshold. In order to optimize the design of the modules and the associated light guides, dedicated attenuation measurements and simulations of the light propagation in the scintillator were undertaken. The light attenuation curve was measured by integrating the anode pulses arising from the excitation of the plastic scintillator by a light generator placed at different positions along the scintillator.

Preliminary test measurements with an NE102 plastic scintillator bar, 80x12x4 cm^3, with wedge shaped plexiglass light guides, exhibited an attenuation curve with a region of constant attenuation more then 60 cm long. Such an effect means that the length of the scintillator can be increased without further affecting the light collection. Due to the overall weight, flight path and mechanical integrity a length of 160 cm was finally chosen for the modules. The ends of the modules are wedge shaped tappering down to the PMT's, thus obviating the need for light-guides. By removing the surface of contact between a separate light-guide and the scintillator the amount of light attenuation is reduced, as well as increasing the area of active scintillator. Fig. 2 shows the attenuation curve measured for one such module, both prior to and following being curved to a radius of 120 cm.

and then cooling them very slowly to room temperature.

2.3 Final design

The final overall design chosen for the TONNERRE array is shown in Fig. 1. The array consists of 32 elements, BC400 plastic scintillators, each element having the shape and dimensions shown in Fig. 4.

The scintillators were wrapped in aluminum foil 10 μm thick and in a black plastic foil of 150 μm thickness. As each module is viewed at both ends by two PMT's, the requirement of an event registered in both significantly reduces the contribution due to noise, whilst the time difference provides for a determination of the position of the event along the detector. The contact between the PMT and the scintillator is assured by a disk of Plasmol, 3 mm thick and 50 mm diameter. Plasmol is a silicon elastomere [2] which is elastic, resistant and has excellent optical properties. The light transmission coefficient at λ=420 nm is 93.2 %. The radius of curvature for the scintillators and the neutron flight path is 120 cm. The solid angle covered by a single module is 0.2 sr. Each detector module is supported between two curved aluminum plates, 5 mm thick which also secure in place the two PMT's. The modules may be mounted on a chassis (Fig. 1) in a variety of configurations, as dictated by the individual experiments. The start for the TOF measurement is provided by the detection of the decay electrons in an implantation detector, an NE102 plastic scintillator block, 3x3x1 cm^3 viewed by two PMT's.
The characteristics of the array, as described in the following section, have been determined experimentally via preliminary source tests and in-beam measurements at GANIL.

3 Test measurements using radioactive sources

Individual detector modules have been tested using a β^- source of $^{90}Sr(^{90}Y)$ and a ^{252}Cf neutron source. The light pulses arriving at the PMT's were analysed in amplitude and time: E_1, t_1 from the left side and E_2, t_2 from the right side (Fig. 5).

Here t_1 and t_2 are the arrival times at the PMT's. In the case of the β-source, the start signal was given by a third PMT coupled with a 0.5 mm thin NE102 plastic scintillator placed between the source and the module. In the case of

[2] †Rhodersil silicones, produced by Rhône Poulenc

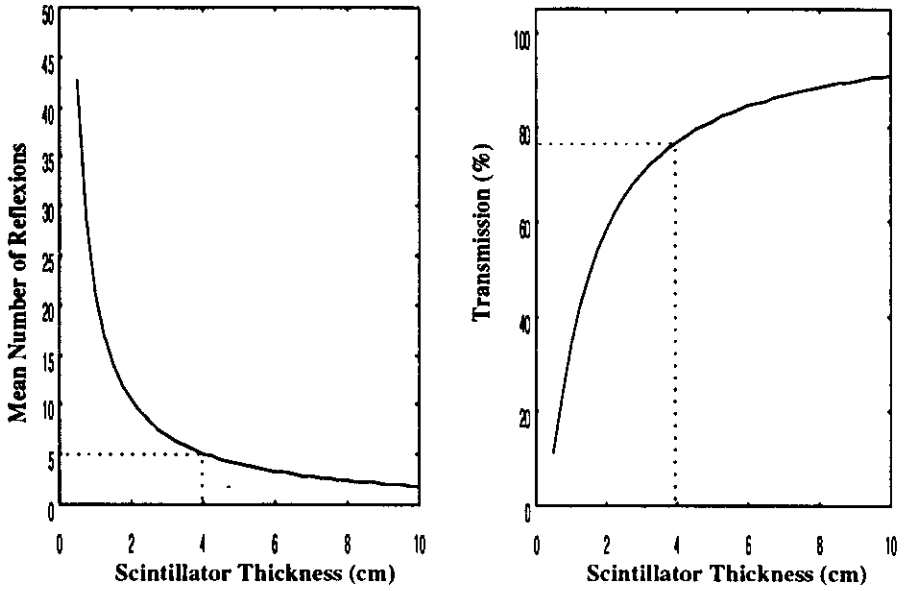

Fig. 3. Calculated number of reflections and the ratio of transmitted to emitted light as a function of scintillator thickness.

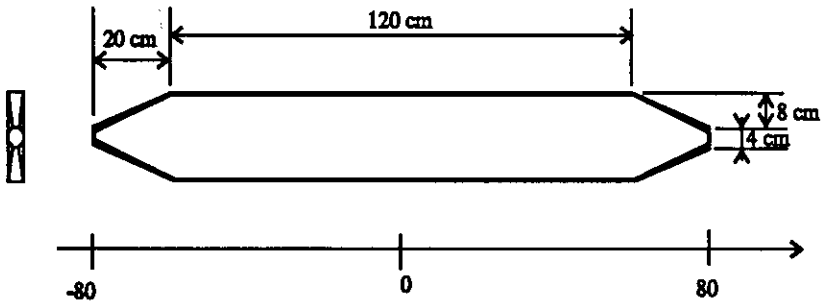

Fig. 4. Design chosen for the individual scintillator modules.

Finally the code Guide7 was employed in order to optimize the dimensions of the wedge shaped light-guide (in particular the length) so that the light transmission is optimum. For a scintillator with a total length of 160 cm and a cross-section of 20x4 cm^2, the length of the guide was varied between 10 and 30 cm. The light attenuation was defined as the ratio between the maximum amplitude of the transmitted light, corresponding to an emission point close to the PMT and the minimum amplitude, corresponding to the emission point in the middle of the scintillator. The simulations show that the attenuation is minimum for a length of 20 cm.

Fig. 4 shows the final shape chosen for the scintillator modules following the simulations and test measurements described above.

The modules were delivered by Bicron as flat bars. They were subsequently curved to a radius of curvature of 120 cm in a basin of water having a curved bottom of radius 124 cm, by heating them to a softening temperature of $75°C$

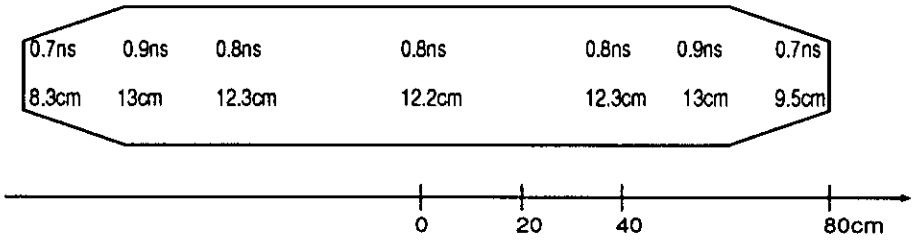

Fig. 6. Time and position resolutions for different positions along the scintillator module.

3.2 Time and position resolution

For these measurements the β-source was again used. The time resolution δ_{t_1}, δ_{t_2} is defined by the FWHM of the time spectra taken with PM1(t_1) and PM2(t_2) (Fig. 5). By measuring δ_{t_1} and δ_{t_2} we can determine the TOF resolution, as, from (4) and (5) it follows that,

$$TOF = \frac{t_1 + t_2}{2} - \frac{l}{2v} \tag{6}$$

Consequently the mean, global TOF resolution is,

$$\delta_{TOF} = \frac{1}{2}\sqrt{\delta_{t_1}^2 + \delta_{t_2}^2} \tag{7}$$

In order to determine the position, X, of impact along the scintillator (Fig. 5) the two pairs of signals E_1, t_1 and E_2, t_2 were used. Several localisation functions were tried. The best position resolution was obtained by,

$$X = offset + slope * \frac{t_1 - t_2}{t_1 + t_2} \tag{8}$$

The position resolution was defined as the FWHM of the X spectrum. The TOF and position resolutions were determined for different locations along the scintillator. The results are shown in Fig. 6.

The two resolutions change with position along the scintillator but do not depend on the transverse position of the source. The best TOF and position resolutions were obtained when the source was positioned in the wedge shaped "light guide".

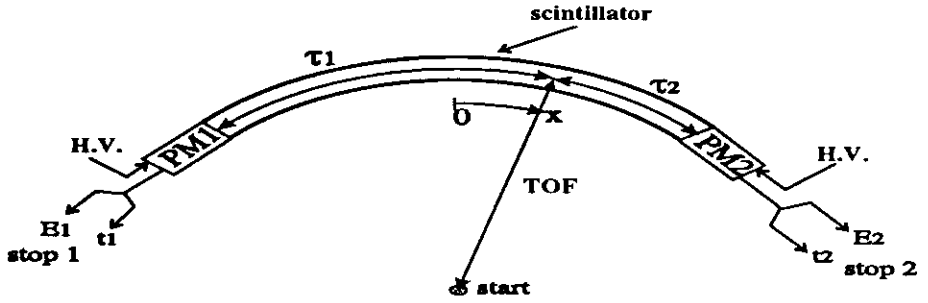

Fig. 5. A schematic view of the experimental arrangement for testing the characteristics of individual modules using radioactive sources.

^{252}Cf (a spontaneus fission source), the start signal was provided by the fission fragments detected in a surface-barrier detector.

3.1 Light speed inside the scintillator

Fig. 5 shows the relationship between the measured times, t_1, t_2 and the TOF,

$$t_1 = TOF + \tau_1; \qquad t_2 = TOF + \tau_2 \tag{4}$$

where τ_1 and τ_2 are the propagation times inside the scintillator. Of course,

$$\tau_1 + \tau_2 = \tau = l/v \tag{5}$$

where l is the scintillator length and v is the speed of light inside the scintillator. By positioning the β-source close to the detector, τ_1 and τ_2 are identical with the measured times t_1, t_2 and from (5) we determined the light speed in the scintillator to be 16.3 cm/ns. Knowing the refractive index to be 1.58 (specified by BICRON), the calculated speed is 19 cm/ns. The difference is due to the light reaching the PMT by multiple reflections which increases the optical path beyond the geometrical distance between the scintillation point and the PMT. Indeed, the apparent speed of 16.31 cm/ns is in agreement with a previously determined value of 16.7 cm/ns for a scintillator of 3 cm thickness [20].

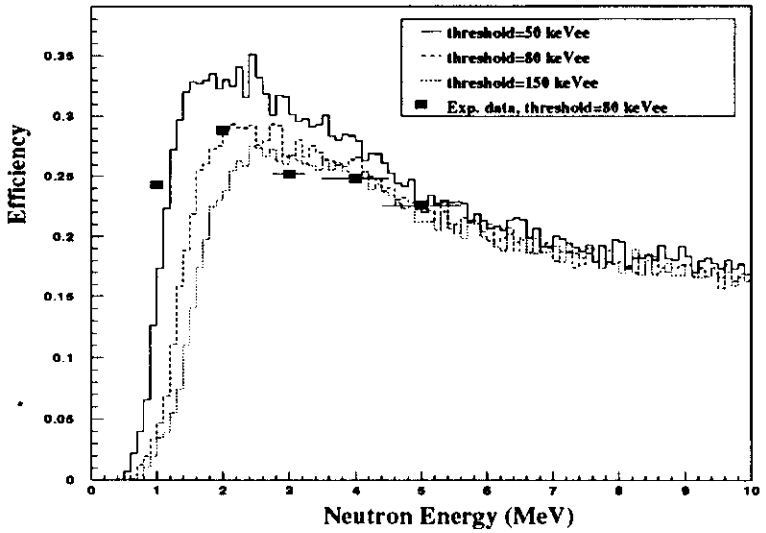

Fig. 8. Measured intrinsic efficiency for a single module using the ^{252}Cf source and a threshold of 80 keVee (full points). The curves are calculated efficiencies for various thresholds, using the code GEANT.

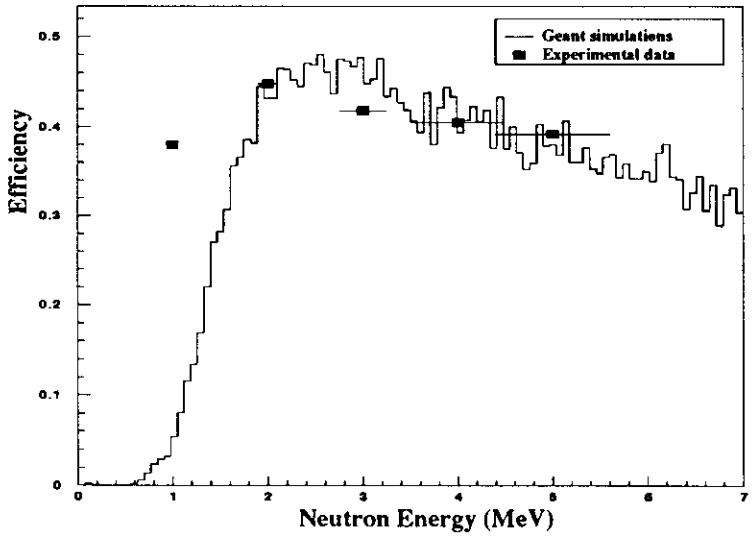

Fig. 9. The same as Fig. 8, but for two scintillators stacked together.

4 Beam tests

In-beam tests have also been performed at GANIL, Caen, in order to measure the β-delayed neutron energy spectra of a number of known nuclei. The main goal of this study was to establish the energy resolution (only possible with discrete line sources), verify the intrinsic detection efficiency and determine the

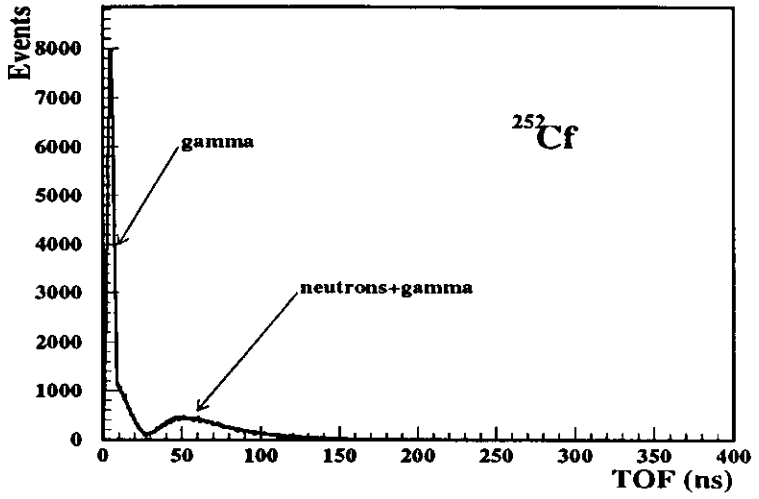

Fig. 7. TOF spectrum for neutrons from a ^{252}Cf source for a single scintillator module.

3.3 Intrinsic detection efficiency

A series of measurements were undertaken to establish the intrinsic neutron detection efficiency of a module as a function of energy. The arrangement used was that displayed in Fig. 5, where the β^- source was replaced by the ^{252}Cf source (3.67 neutrons emitted per fission event [21]) positioned at the center of the radius of curvature.

From the TOF spectrum of Fig. 7 the number of neutrons detected over each energy interval, and thus the efficiency, could be determined.

It is well known that the efficiency depends on the threshold for light collection (expressed in electron equivalent energy). The intrinsic efficiency of one module, as calculated using the GEANT code, is shown in Fig. 8 for three different thresholds. For the threshold of 80 keVee, which was used in the experiment, there is a good agreement between the experimental values and the simulation, except for the point at 1 MeV.

Measurements have also been made for two detectors stacked together (Fig. 9). The efficiency of this combination is very high, of the order of 42% for a threshold of 80 keVee. The agreement with the simulations is quite good up to 5 MeV. For higher energies the yield from the ^{252}Cf source became too low for reliable measurements.

Table 1
Energies of β-delayed neutrons for the nuclei studied here. The corresponding branching ratios are noted in parentheses.

Nucleus	E_n(MeV) / BR				
^{15}B[11]	1.76	2.82	3.20	4.33	4.82
	(0.629)	(0.079)	(0.229)	(0.041)	(0.019)
^{16}C[22]	0.80	1.72			
	(0.84)	(0.16)			
^{17}N[23]	0.38	1.16	1.69		
	(0.380)	(0.501)	(0.069)		

A primary beam of ^{18}O, 77A MeV, and a thick (4000 μm) Be target were employed to produce secondary beams of ^{15}B, ^{16}C and ^{17}N. Beam purification was achieved using LISE coupled with an achromatic degrader.

Table 1 lists the β-delayed neutron energies for the measured nuclei. These groups and the corresponding branching ratios have been used to determine the energy resolution and detection efficiency as a function of neutron energy.

4.1 Energy resolution and intrinsic efficiency

As an example we show in Fig. 11 the TOF and energy spectrum of β-delayed neutrons from the decay of ^{15}B.

In Fig. 11 the energies (MeV) of the corresponding lines as calculated from the measured TOF are indicated with arrows. The shape of the lines in the TOF spectrum are somewhat asymetric (in Fig. 11 we show a fit using asymetric gaussians), having tails which extend to lower energies. These tails arise principally from neutrons which have been detected with low deposited charge.

The energy spectrum of β-delayed neutrons from ^{17}N is displayed in Fig. 12. The detection of the group at 0.38 MeV demonstrates that TONNERRE is capable of operating at quite low thresholds ($\sim$ 300 keV) despite its thickness.

The energy dependence (Table 2) of the resolution (FWHM) has been determined by interpolating between the values obtained for various peaks (Table 1) observed in the decays of ^{15}B, ^{16}C and ^{17}N .

The major factor contributing to the final energy resolution ($\delta E/E \sim 10\%$) arises from the uncertainty in the flight path (see eq. 1). This uncertainty

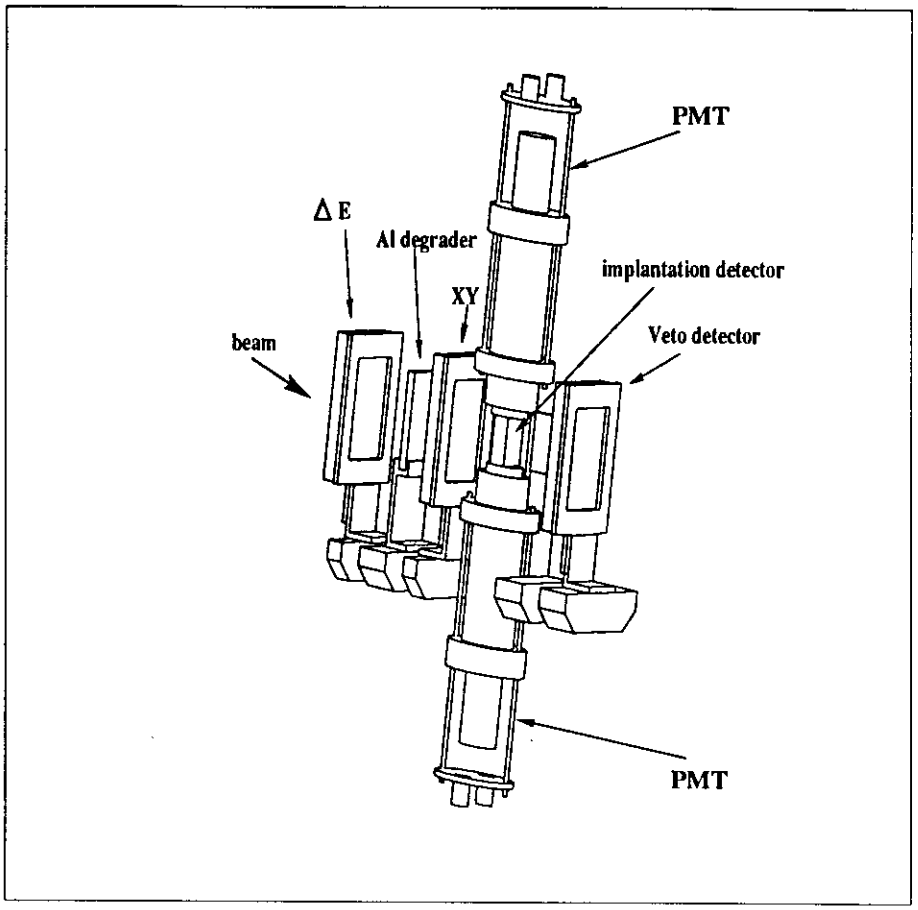

Fig. 10. The elements of the telescope used for in-beam testing.

performances of the array under beam conditions. For these tests TONNERRE was installed at the final focus of the LISE3 spectrometer [6]. The 32 detector modules were arranged in two layers, 23 in the first layer and 9 in the second. A detector telescope which provided for ion identification, collection and β-detection was located at the centre of the array. The telescope, shown in Fig. 10 consisted of 4 active elements and a degrader.

- A 5x5 cm^2, 300μm thick, Si surface barrier detector (ΔE) for particle identification by the ΔE-TOF method.
- An aluminum degrader with the thickness chosen such that the ions of interest were stopped in the middle of the implantation detector.
- A Si, XY position sensitive detector, 5x5 cm^2 and 300 μm thick, which allowed the beam dimensions and position to be monitored.
- An implantation detector, which consisted of an NE102A plastic scintillator block, 3x3x1 cm^3, viewed by two XP2972 PMT's, for detection of the decay β's.
- A Si surface barrier veto detector, 5x5 cm^2 and 500μm thick.

Table 2
Experimental energy resolution

Energie(MeV)	1	2	3	4	5
$\delta_E/E(\%)$	10.3	10.6	10.8	11.1	11.3
FWHM (keV)	103	212	318	444	565

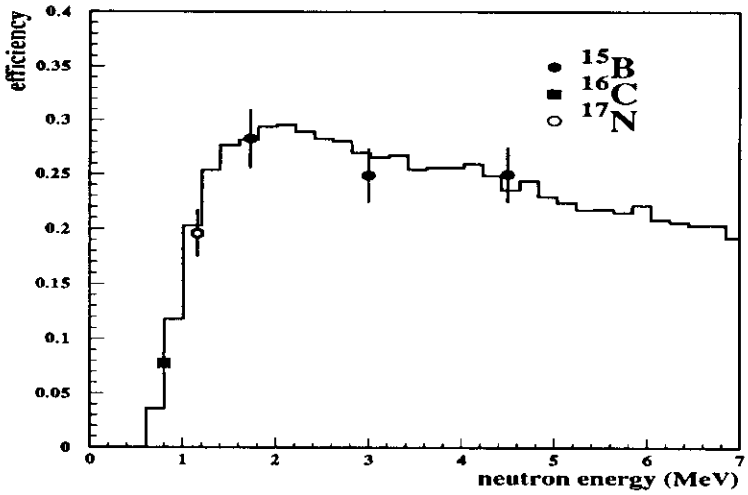

Fig. 13. Experimentally determined intrinsic efficiency of a single module obtained from the in-beam tests (points). The histogram represents the efficiencies calculated using the code of Cecil *et al* [24].

includes: a contribution from the thickness of the detector modules (4 cm); the dimension of the beam spot on the implantation detector ($\sim$ 1.5 cm in diameter) and deviations along the module from the nominal 120 cm radius of curvature. We note that the limiting factor amongst these contributions is the detector thickness ($\delta E/E \sim 8\%$).

By comparing the number of detected β-decays in the implantation detector and the number of implanted ions (counted using the Si telescope), an average β-detection efficiency of 90 % was determined for β-energies ($E_\beta \leq 20$ MeV) of the nuclei studied here. The β-detection efficiency, together with the known branching ratios have been used to determine the intrinsic efficiency for each detector module as a function of neutron energy. The results obtained for a single module are shown in Fig. 13.

In this figure the continuous curve are calculated efficiencies using the code of Cecil *et al* [24]. For clarity, when two neutron lines were close together (less than 500 keV), the averaged efficiency has been plotted for the mean energy.

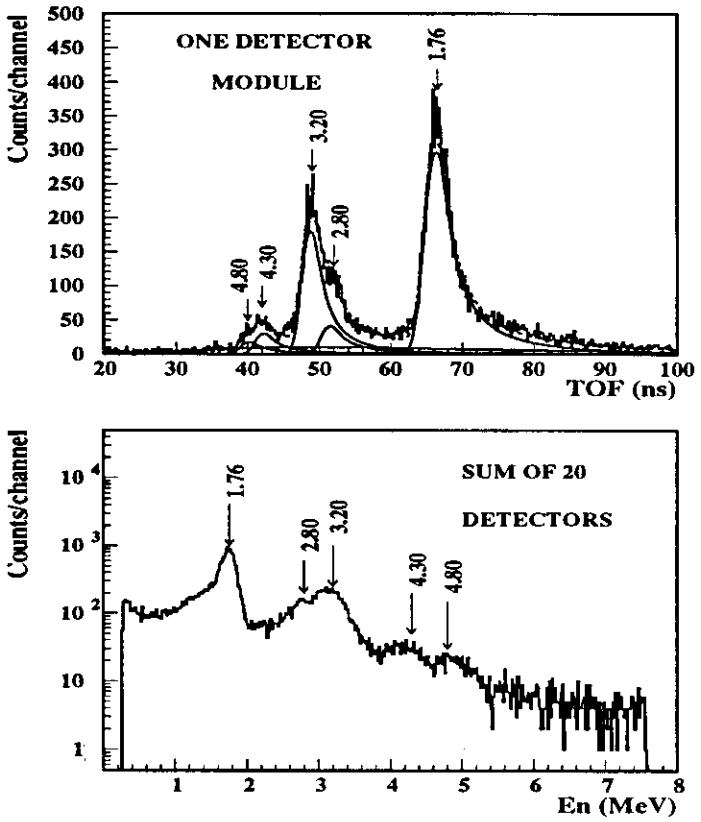

Fig. 11. TOF and energy spectrum of β-delayed neutrons from ^{15}B. The curves are fits employing asymmetric gaussians.

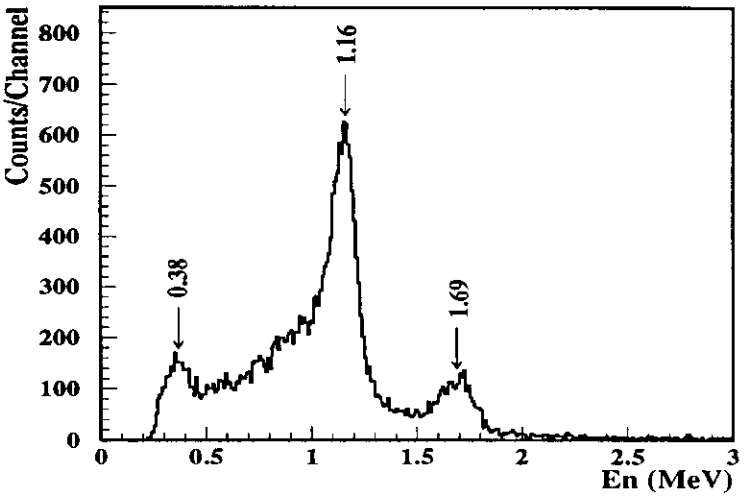

Fig. 12. Energy spectrum of β-delayed neutrons from ^{17}N.

Table 3
Predicted out-scattering and cross-talk for 5 MeV neutrons and a threshold of 80 keVee.

$\phi(^o)$	Out-scattering(%)	Cross-talk(%)	Ω(% of 4π)	No. of detectors
13	0.29	0.10	45	28
26	0.12	0.03	22.2	14
39	0.10	0.019	14.3	9
52	0.04	0.01	9.5	6

Table 4
Cross-talk probability calculated with GEANT for a threshold of 80 keVee and extracted from in-beam measurements (^{15}B).

Neutron energy (MeV)	Two detectors side by side		Two detectors superimposed	
	GEANT	measured	GEANT	measured
1.76	0.033%	0.049±0.017%	0.30%	0.23±0.08%
2.82/3.20	0.055%	0.090±0.033%	1.50%	0.90±0.34%
4.33/4.82	0.100%	0.175±0.090%	2.26%	1.71±0.92%

able. From Table 4 it is clear that, in order to minimize the effect of cross talk, the measurements of multi-neutron decays (with probabilities of the order of few percent or less) should be done with the detectors arranged side-by-side.

5 Summary and Conclusions

The main characteristics of TONNERRE are summarized in Table 5 together with the characteristics of similar multi-detector arrays for delayed neutron spectroscopy in operation elsewhere. We note that with a high overall efficiency of 15 % and high granularity, TONNERRE is well placed to undertake a competitive programme of delayed-neutron decay spectroscopy.

In conclusion, we have reported on the design and construction of a multi-detector array dedicated to β-delayed neutron decay spectroscopy. The array consists of 32 plastic scintillator modules, 160x20x4 cm^3, bent to a radius of curvature of 120 cm and viewed at both ends by PMT's which allow for TOF and position measurements. The 32 detector modules can be arranged in different geometries and in one or two layers, depending on the experimental requirements. The start for the TOF measurements is given by the β-rays detected in an implantation detector positioned at the center of the array.

4.2 Cross-talk

The detector modules of TONNERRE, as described in section 2 are mounted on a chassis in a configuration which depends on the experiment. The number of detectors which can be arranged in one layer in order to cover the maximum solid angle (45% of 4π) is 28. Unfortunately, mounting the detectors close together can complicate the analysis by enhancing the effects of cross-talk and out-scattering-the former being of particular importance when studying multi-neutron emission. Cross-talk is the familiar problem of one neutron being detected in two separate detectors. Out-scattering may arise when a neutron scatters from a non-active part of the array and is subsequently detected (with an erroneous position and TOF) or when a neutron is scattered from a module without being detected (the energy deposited did not exceed the threshold) and is detected in a second detector.

While methods exist for identifying and eliminating cross-talk events [25], there are no methods available for identifying out-scattered events. Therefore, the array should contain as little non-active material as possible. As noted earlier, the frames which hold and ensure the mechanical integrity of each scintillator are composed of two aluminum plates, each of them 5 mm thick (Fig. 1). Compared to the 20 cm width of each module, the supports represent an inactive area of only 5% of the total area.

From a practical view point, due to their low absolute counting rates out-scattering and cross-talk will have, in general, negligible effect on the single-neutron energy spectra. Cross-talk on the other hand, is potentially of great importance in the detection of two- or three- neutron decays which typically occur with low branching ratios. The solutions to reduce the cross-talk and outscattering imply rather high costs. Increasing the detection threshold translates directly to a reduction in the intrinsic efficiency. Similarly, increasing the distance between the detectors reduces the geometric efficiency.
In Table 3, the simulated probabilities for cross talk and outscattering are listed for various angular separations (ϕ) of the modules. The simulations considered only the interactions between neighbouring detectors and were performed for a neutron energy of 5 MeV.

The counting rate for both effects decreases as the angle ϕ is increased whilst the overall geometrical efficiency of the array decreases. For example, retaining only one out of every two detectors reduces the cross-talk by a factor of three. However the angular coverage is decreased by 50%.

The rates of cross-talk have been derived from the in-beam tests with ^{15}B (Table 4) for two detectors side-by-side and superimposed.

The agreement between measurements and simulations in Table 4 is reason-

Acknowledgements

The realisation of TONNERRE was done in the frame of "Programme International de Cooperation Scientifique" (IN2P3-NIPNE) and the support of some of us (CB, AB, IC, FN, CS and CT) through this PICS is gratefully acknowledged.
We would like to thank the technical staff of LPC-Caen and NIPNE-Bucharest for designing and constructing the mechanical structure of TONNERRE. The assistance and support provided by the staffs of LPC-Caen and LISE3-GANIL during the beam tests is also gratefully acknowledged.

References

[1] B. Jonson and G. Nyman,

In, *Nuclear Decay Modes*, 1996, p. 102,
Edited by D.N. Poenaru, Institute of Physics Publishing, Bristol and Philadelphia.

[2] D. Bazin, A.C. Mueller, and W.D. Schmidt-Ott, *Nucl.Instr. Meth.*, **A281** (1989) 117

[3] A.C. Mueller, D. Bazin, W.D. Schmidt-Ott, R. Anne, D. Guerreau, D. Guillemaud-Mueler, M.G. Saint-Laurent, V. Borrel, J.C. Jacmart, E. Pougheon and A. Richard,*Z. Phys.*, **A330** (1988) 63

[4] A.C. Mueller, D. Guillemaud-Mueller, J.C. Jacmart, E. Kashy, F. Pougheon, A. Richard, A. Handt, H.V. Klapdor-Kleingrothaus, M. Lewitowicz, R. Anne, P. Briault, C. Detraz, Yu.E. Penionzhkevich, A.G. Artukh, A.V. Belozyarov, S.M. Lukyanov, D. Bazin and W.D. Schmidt-Ott, *Nucl. Phys.*, **A513** (1990) 1

[5] M. Lewitowicz, Y.E. Penionzhkevich, A.G. Artukh, A.M. Kalinin, V.V. Kamanin, S.M. Lukyanov, Nguen Hoai Chan,A.C. Mueller, D. Guillemaud-Mueller, R. Anne, D. Bazin, C. Detraz, D. Guerreau, M.G. Saint-Laurent, V. Borrel, J.C. Jacmart, F. Pougheon, A. Richard and W.D. Schmidt-Ott, *Nucl. Phys.*, **A496** (1989) 477

[6] R. Anne and A.C. Mueller, *Nucl. Instr. Meth. Phys. Res.*, **B70** (1992) 276

[7] J.P. Dufour, R. Del Moral, F. Hubert, D. Jean, M.S. Pravikoff, A. Fleury, A.C. Mueller, K.H. Schmidt, K. Summerer, E. Hanelt, J. Frehaut, M. Beau and G. Giraudet, *Phys. Lett.*, **B206** (1988) 195

[8] P.L. Reeder, R.A. Warner, W.K. Hensley, D.J. Vieira and J.M. Wouters, *Phys. Rev.*, **C44** (1991) 1435

Table 5
Parameters and performances of various β-delayed neutron detectors. R: the flight path (in the case of the RIKEN "Wall" a typical distance is given, for which the flight path is measured with respect to the center of the detector). d: the scintillator thickness. $\Delta\Omega$: solid angle-fraction of 4π. ϵ_n: intrinsic efficiency for 2 MeV neutrons. ΔE_n: energy resolution (FWHM) for 1 MeV neutrons. Δx: position resolution along one module. $\Delta\Omega.\epsilon_n$: the overall efficiency (for TONNERRE the overall efficiency corresponds to a configuration with 28 modules in the first layer and 4 modules in the second).

Array (Scintillator)	Nr. of elements	R (m)	d (cm)	$\Delta\Omega$	ϵ_n	ΔE_n (keV)	Δx (cm)	$\Delta\Omega.\epsilon_n$
MSU [11] (BC412)	16	1.00	2.5	15%	20%	50	13	3%
RIKEN "Wall" [16] (BC408)	15	1.25	6.0	11%	55%	110	7	6%
RIKEN[15] (BC408)	6	1.50	2.0	10%	20%	50	-	2%
IRES [10] (NE110)	1 1	1.00 1.00	5.00 1.25	2.29% 2.29%	36% 9%	- -	- -	0.82% 0.2%
TONNERRE (BC400)	32	1.20	4.0	45%	30%	103	12	15%

The tests undertaken with a neutron source and with beams of known neutron-rich nuclei have demonstrated that the array has simultaneously, good energy resolution ($\sim$ 10% for neutrons up to 5 MeV), a high intrinsic efficiency ($\sim$ 30% for 2 MeV neutrons) and a large acceptance (up to 50% of 4π). The array operates with a relatively low threshold ($\sim$ 300 keV in neutron energy) and it is envisaged that it may be complemented for decay studies by the addition of high efficiency γ-ray detectors.

Future experimental studies with the array include investigations of the N=20 [26] and N=28 [27,28] shell closures along with an exploration of the spectroscopy of neutron-rich A$\sim$ 20 nuclei [29].

[27] H. Scheit, T. Glasmacher, B.A. Brown, J.A. Brown, P.D. Cottle, P.G. Hansen, R. Harkewicz, M. Hellström, R.W. Ibbutson, J.K. Jewell, K.W. Kemper, D.J. Morrissey, M. Steiner, P. Thirolf and M. Thoennessen, *Phys. Rev. Lett.*, **77** (1996) 3967

[28] O. Sorlin, D. Guillemaud-Mueller, A.C. Mueller, V. Borrel, S. Dogny, F. Pougheon, K.L. Kratz, H. Gabelmann, B. Pfeiffer, A. Weller, W. Ziegert, Y. Penionzhkevich, S.M. Lukyanov, V.S. Salamatin, R. Anne, C. Bonn, L.K. Fifield, M. Lewitowicz, M.G. Saint-Laurent, D. Bazin, C. Detraz, F.-K. Thielemann and W. Hillebrandt, *Phys. Rev.*, **C47** (1993) 2941

[29] see, for example, D. Bazin, W. Benenson, B.A. Brown, J. Brown, B. Davids, M. Fanerbach, P.G. Hansen, P. Mantica, D.J. Morrissey, C.F. Powell, B.M. Sherrill and M. Steiner, *Phys. Rev.*, **C57** (1998) 2156, and ref's therein